J. Mol. Biol. (1996) **263**, 369–382

JMB

Contributions to Conformational Entropy Arising from Bond Vector Fluctuations Measured from NMR-Derived Order Parameters: Application to Protein Folding

Daiwen Yang* and Lewis E. Kay*

Protein Engineering Centers of Excellence and Departments of Medical Genetics, Biochemistry and Chemistry, University of Toronto, Toronto, Ontario Canada, M5S 1A8

**Corresponding authors*

The relation between order parameters derived from NMR spin relaxation experiments and the contribution to conformational entropy from ns-ps timescale bond vector dynamics is investigated by considering a number of simple models describing bond vector motion. In a few cases both classical and quantum mechanical derivations are included to establish the validity of obtaining order parameter-entropy relations using classical mechanics only. For these cases it is found that classical and quantum mechanical derivations give very similar results so long as the square of the order parameter of the bond vector is less than ~ 0.95. For a given change in order parameter, the change in conformational entropy is sensitive to the model employed, with the absolute value of the entropy change increasing with the number of degrees of freedom in the model. The entropy-order parameter profile calculated from a 1.12 ns molecular dynamics trajectory of fully hydrated *Escherichia coli* ribonuclease HI is well fit using a simple expression based on a model assuming bond vector diffusion in a cone, suggesting that it may well be possible to extract meaningful entropy changes reflecting changes in ps-ns time scale motions from changes in NMR-derived order parameters. Contributions to the conformational entropy change associated with a folding-unfolding transition of an SH3 domain and calculated from changes in rapid $N\text{-}H^N$ backbone dynamics are presented.

Keywords: NMR spin relaxation; order parameters; conformational entropy; protein folding

Introduction

Many biological processes, including protein folding, intermolecular protein-protein interactions and protein-ligand interactions, are accompanied by potentially significant entropy and enthalpy changes (Duntz 1995; Lee *et al*., 1994; Weber, 1995; Brooks *et al*., 1988; Schellman. 1987). An understanding of the stability and function of biomolecules requires a description of the three-dimensional structures of such molecules, knowledge of their thermodynamic parameters and how such parameters vary upon a change of conditions (e.g. ligand binding). Experimentally, global thermodynamic values that characterize a net change in the system associated with a transition between two states have been measured from optical methods (Schmid, 1989; Viguera *et al*., 1994) such as circular dichroism and fluorescence or by calorimetric approaches (Plum & Breslauer, 1995) such as scanning and titration calorimetry. Recently Markley and co-workers (Dzakula *et al*., 1992a,b, 1996) have developed a method for analyzing rotamer populations from NMR spin-spin couplings and nuclear Overhauser (NOE) enhancements. In favorable cases this approach allows the characterization of the thermodynamics of internal rotation. On the theoretical side, molecular dynamics and Monte Carlo simulations in principle allow estimation of thermodynamic parameters in some

Abbreviations used: A, Helmholtz free energy; Ndrk SH3, amino-terminal SH3 domain from the protein drk; NMR, nuclear magnetic resonance; $p(j)$, probability density function for bond j; S, entropy; S_{LZ}, order parameter; Z, partition function; $z(j)$, NMR observable contribution to the partition function from bond vector j.

0022–2836/96/420369–14 $25.00/0

detail and offer the possibility of localizing changes in such values to particular sites in the molecule (Brooks *et al*., 1988; McCammon & Harvey, 1987). However, extraction of meaningful values from such simulations does require the use of accurate force-fields, simulations of sufficient length and care that the system under study is in equilibrium (van Gunsteren, 1993).

NMR spin relaxation experiments can provide important information about molecular dynamics extending over a wide range of timescales (Palmer, 1993; Dayie *et al*., 1996; Wagner, 1993). With the recent development in heteronuclear, multi-dimensional NMR it has become possible to obtain motional information about a large number of sites in a labeled molecule (Nirmala & Wagner, 1988, 1989; Kay *et al*., 1989). A significant number of studies have appeared in the literature making use of ^{15}N and ^{13}C spin relaxation methods to study backbone dynamics (Clore *et al*., 1990; Stone *et al*., 1992; Kordel *et al*., 1992; Peng & Wagner, 1992; Nicholson *et al*., 1995; Farrow *et al*., 1994) and more recently an approach for studying side-chain dynamics in proteins was described employing ^{2}H relaxation measurements (Muhandiram *et al*., 1995; Kay *et al*., 1996). Heteronuclear relaxation experiments typically provide heteroatom T_1 and T_2 relaxation values as well as steady-state heteronuclear nuclear Overhauser enhancements. These measurables are subsequently interpreted in the context of motional models. A particularly powerful approach is the so-called ''model-free'' analysis described by Lipari & Szabo (1982a,b), which in its simplest form allows extraction of an overall rotational correlation time, a correlation time that characterizes internal dynamics and an order parameter that describes the amplitude of the internal motions from NMR relaxation time measurements.

Very little literature has appeared on the relation between thermodynamic parameters such as entropy and parameters derived from NMR relaxation experiments. However, as we describe in more detail below, both the entropy and the order parameter of a bond vector depend on the distribution of orientations of the vector and it is therefore possible to derive a relation between changes in order parameter and changes in entropy, providing this distribution is known. The advantage of linking changes in NMR-derived parameters to changes in thermodynamic quantities is that it becomes possible to determine changes in such parameters at each site for which NMR-derived information is available. Akke *et al*. (1993) recognized this advantage and in an important recent paper those authors related free energy changes to changes in NMR-derived order parameters. In addition, the authors applied the method to calculate energy changes, on a per-residue basis, that occur upon ion binding to the protein calbindin D_{9k}.

Here, we consider a system undergoing a transition between two states, a and b and derive a relation between conformational entropy changes and changes in NMR-derived order parameters that accompany this transition. Because the order parameters reflect only on rapid ps-ns timescale dynamics, only the contributions to conformational entropy derived from these motions can be calculated. We show that although for certain classes of motional models the calculated entropy change associated with an order parameter change is reasonably independent of the model considered, in general extraction of meaningful changes in entropy requires a knowledge of the motional properties of the bond vector under consideration. In order to establish whether a particular motional model can approximate motions in proteins, we have examined a 1.12 ns molecular dynamics trajectory of fully solvated *Escherichia coli* ribonuclease HI (Philippopoulos & Lim, 1995). The results indicate that the conformational entropy *versus* order parameter profile calculated for backbone $N\text{-}H^N$, $C^\alpha\text{-}H^\alpha$ and side-chain $N\text{-}H^N$ bond vectors in the protein is extremely well approximated by the profile obtained assuming a diffusion-in-a-cone model. On the basis of these results, we estimate the contributions to the change in conformational entropy from ps-ns time scale motions, on a per-residue basis, that occur upon folding of an SH3 domain.

Theory

Statistical mechanics provides a powerful approach for connecting macroscopic properties of a given system such as the Helmholtz free energy, A, or the entropy, S, with its microstates (Nash, 1974). In the case of S and A this can be accomplished by noting that:

$$S = -(\partial A / \partial T)v \tag{1}$$

and

$$A = -kT \ln Z_{TOT} \tag{2}$$

where T is the absolute temperature, k is Boltzmann's constant and Z_{TOT} is the partition function of the system from which it is possible to evaluate all of its essential thermodynamic properties. Assuming that all of the molecules in the system are completely uncoupled (i.e. that no force acts between the molecules), Z_{TOT} can be written as

$$Z_{TOT} = Z^N / N! \tag{3}$$

where N is the number of identical molecules, Z is the molecular partition function, and the factor $N!$ corrects for overcounting the number of distinguishable states in a system of N identical molecules, assuming Boltzmann statistics (Nash, 1974). Z can be further factored into a product of partition functions, each of which describes statistically independent degrees of freedom within each molecule. Accordingly, we write:

$$Z = Z_U Z_O, \tag{4}$$

where Z_O is the contribution to Z arising from bond vector fluctuations that can be measured in NMR relaxation experiments and Z_U is the remaining contribution from all other sources. Finally, under the further assumption that each fluctuating bond vector is independent of all others, it is possible to recast equation (4) as:

$$Z = Z_U \prod_j z(j) \tag{5}$$

where the product extends over all j bond vectors in the molecule and the partition function, $z(j)$ is given by:

$$z(j) = \Sigma_i \exp\{-E_i(j)/(kT)\}. \tag{6}$$

In equation (6) the summation includes all of the energy states, E_i, of the bond vector. Note that the assumption of independence of bond vector motions can result in an over-estimate of the value of the partition function (Akke *et al*., 1993). Thus the methodology described will yield upper-bounds on the thermodynamic parameters calculated from $z(j)$. The validity of the assumptions implicit in equations (4) and (5) is discussed further below. The total entropy of the system, S_{TOT}, can be calculated from equations (1), (2) and (5) according to:

$$S_{TOT} = N(S_U + S_O) - k \ln N! \tag{7.1}$$

$$S_O = \Sigma_j \partial\{kT \ln z(j)\} / \partial T \tag{7.2}$$

$$S_O(j) = \partial\{kT \ln z(j)\} / \partial T \tag{7.3}$$

where S_O and S_U are the contributions to the total entropy per molecule from motions that either are or are not observed in NMR relaxation experiments, respectively, and $S_O(j)$ is the component of S_O arising from bond j. Equation (7.3) indicates that once the partition function, $z(j)$, is calculated it is straightforward to estimate $S_O(j)$.

The partition function can be calculated in a number of different ways, depending on whether a classical or quantum mechanical treatment of the problem is used. In the quantum formulation $z(j)$ is derived directly from equation (6) and the quantized energy states E_i must be known. The entropy for the jth bond can then be calculated directly from equations (6) and (7.3) to give:

$$S_O(j)/k = -\Sigma_i p_i(j) \ln\{p_i(j)\} \tag{8}$$

where $p_i(j)$ is the well-known Boltzmann equation given by:

$$p_i(j) = \exp\{-E_i(j)/(kT)\} / \Sigma_i \exp\{-E_i(j)/(kT)\} \tag{9}$$

In contrast, the classical approach assumes that there is a continuum of states, such that the energy difference between any two successive states is much less than kT. In this case, the summation of energy states, E_i, in equation (6) can be replaced by the integral (Hill, 1986; Fowler & Guggenhein, 1965):

$$z(j) = h^{-L} \int_{pL,qL} \exp\{-E_j(p, q)/(kT)\} dp^L dq^L \tag{10}$$

where p and q are the momenta and coordinates of the particles that comprise the bond vector in question (see Methods), L is the number of degrees of freedom and $E_j(p, q)$ is the energy of bond j. In what follows the subscript j is omitted.

It is straightforward to show that for both one (1D) and two-dimensional (2D) internal rotation the partition function can be written as:

$$z(j) = f(T) \int_v \exp\{-U(q)/(kT)\} dv, \tag{11}$$

where $dv = d\phi$ (1D) or $dv = \sin\theta\, d\theta\, d\phi$ (2D) and $f(T)$ is given by $(1/h)(2\pi IkT)^{0.5}$ and $(1/h^2)(2\pi IkT)$ in the 1D and 2D cases, respectively (see Methods for details). In the Methods section we show that for $z(j)$ given by equation (11) it is possible to write the entropy contribution from rotation of bond vector j as:

$$S(j)/k = \ln f(T) + T\, d\{\ln f(T)\}/dT - \int_v p(q) \ln\{p(q)\} dv \tag{12}$$

where $p(q)$ is the probability density function given by:

$$p(q) = \exp\{-U(q)/kT\} / \int_v \exp\{-U(q)/kT\} dv \tag{13}$$

Note that for the case where $U(q) = 0$, equation (12) becomes:

$$S(j)/k = \ln f(T) + T\, d\{\ln f(T)\}/dT + \ln\{\int_v dv\} \tag{14}$$

Therefore:

$$S(j,U(q))/k - S(j,U(q) = 0)/k = -\int_v p(q) \ln\{p(q)\} dv - \ln\{\int_v dv\} \tag{15}$$

where $S(j,U(q))$ and $S(j,U(q) = 0)$ correspond to the contributions to the entropy from bond vector j in the presence and absence of a potential $U(q)$, respectively. The effect of a non-zero potential, $U(q)$, is to change the entropy of the system by an amount given by the right-hand side of equation (15). Note that the quantity $\ln\{\int_v dv\}$ is independent of $U(q)$ and thus it suffices to consider how the quantity:

$$S_p(j)/k = -\int_v p(q) \ln\{p(q)\} dv \tag{16}$$

changes in the calculation of entropy differences arising from changes in $U(q)$. In what follows we refer to $S_p(j)$ as the conformational entropy. The first two terms in equation (12) are related to the kinetic energy and providing that the kinetic energy does not differ between states a and b, the change in rotational entropy between these two states, $\Delta S(j)$, is equal to $\Delta S_p(j)$. It is instructive to note the analogy between equations (9) and (13). Note that neither $p(q)$ nor $P_i(j)$ depend on the magnitude of the ground state energy, that is:

$$p(q) = \exp\{-U'(q)/(kT)\} / \int_v \exp\{-U'(q)/(kT)\} dv \tag{17.1}$$

$$p_i(j) = \exp\{-E'_i(j)/(kT)\} / \Sigma_i \exp\{-E'_i(j)/(kT)\} \tag{17.2}$$

where $U'(q) = U(q) + U_O$ and $E'_i(j) = E_i(j) + E_O$;

therefore $S(j)$ is also independent of U_O and E_O. This feature is particularly important because it implies that in calculating the entropy change between two states, $\Delta S(j)$, the difference in ground state energies between the two states is insignificant. Unfortunately, this is not the case in the calculation of Helmholtz or Gibbs free energy changes associated with the transition (Akke *et al*., 1993). Finally, it is significant to note that $S(j,U(q)) - S(j,U(q) = 0) \leqslant 0$ for $U(q) \geqslant 0$, since the total entropy of the system must decrease with decreasing degrees of freedom (i.e. as the potential energy increases). Therefore, from equation (15) we can write:

$$S_p(j)/k = -\int_v p(q)\ln\{p(q)\}\mathrm{d}v \leqslant \ln\{\int_v \mathrm{d}v\} \quad (18)$$

Although there is an upper bound for $S_p(j)$ ($S_p(j)/k \leqslant \ln\{2\pi\}$ or $\ln\{4\pi\}$ for 1D or 2D internal rotation, respectively) the value of $Sp(j)$ can indeed be negative, as shown later. However, the total entropy that a given vector contributes to the system, $S(j)$ (i.e. from potential and kinetic energy terms), must always be non-negative; this is illustrated in Methods.

According to the formalism of Lipari & Szabo (1982a, b) it is possible to interpret NMR relaxation parameters in terms of an order parameter, S_{LZ}, which is related to the amplitude of a given bond vector's motion and a number of correlation times describing the timescale of the dynamics. The value S^2_{LZ} is defined according to:

$$S^2_{LZ} = (4\pi/5)\Sigma_r|\Sigma_i p(\theta_i, \phi_i)Y_{2r}(\theta_i, \phi_i)|^2 \quad (19)$$

where $Y_{2r}(\theta_i, \phi_i)$ is a spherical harmonic of rank 2 ($-2 \leqslant r \leqslant 2$), and (θ_i, ϕ_i) are polar angles describing the ith orientation of a bond vector in some molecular coordinate system. Assuming a normalized probability distribution function, $p(q)$, equation (19) can be modified to:

$$S^2_{LZ} = (4\pi/5)\Sigma_r|\int_v p(q)Y_{2r}(q)\mathrm{d}v|^2 \quad (20)$$

in analogy to equations (9) and (13), where $p(q) = p(\phi)$, $Y_{2r}(q) = Y_{2r}(\theta_0, \phi)$ and $\mathrm{d}v = \mathrm{d}\phi$ for one-dimensional internal rotation at an angle of θ_0 about some symmetry axis and $p(q) = p(\theta, \phi)$, $Y_{2r}(q) = Y_{2r}(\theta, \phi)$ and $\mathrm{d}v = \sin\theta\ \mathrm{d}\theta\ \mathrm{d}\phi$ for two-dimensional internal rotation. Note that the order parameter, like $S_p(j)$, depends only on the probability distribution and not on the absolute energy. Inspection of the equations for conformational entropy, S_p, and for S^2_{LZ} suggests that it should be possible to relate the two. To do so, the quantum energy values must be known if a quantum mechanical based description of entropy is to be derived (see equations (6) to (9)) or the potential energy surface must be available if a classical derivation is to be employed (equations (10) and (12)). It is generally the case that a classical calculation of entropy changes from changes in rotational degrees of freedom is adequate (Karplus & Kushick, 1981). Nevertheless, we feel that it is important to include a number of simple examples comparing both quantum mechanical and classical derivations of the S_p *versus* S^2_{LZ} profile to establish the values of S^2_{LZ} for which the classical description breaks down. To the best of our knowledge this question has not been addressed in the literature. A number of examples are illustrated in Methods involving the motion of a bond vector on the surface of a cone, subject to different potential energy functions.

The results in Methods indicate that for $S^2_{LZ} \leqslant 0.95$, classical and quantum mechanical treatments give similar values of entropy. In general, for complicated potential functions, $U(q)$, it is very difficult or impossible to solve the Schroedinger equation to obtain the quantized energy values necessary for a proper quantum mechanical derivation. With this in mind and recognizing the limitations associated with the classical formalism, in what follows we consider a number of different potential functions and evaluate the relation between S^2_{LZ} and the contribution to conformational entropy arising from bond vector fluctuations using the classical approach detailed above and in Methods. This will allow an assessment of how changes in conformational entropy associated with changes in order parameters depend on the model considered.

Results and Discussion

As described in the Introduction, the goal of this work is to develop an approach for relating changes in NMR-derived order parameters to changes in the conformational entropy due to changes in bond vector fluctuations between two states. Unfortunately, the potential surface dictating the trajectory of bond vectors in macromolecules is not known in great detail. Therefore, it is important to establish whether exact knowledge of potential functions is necessary to extract meaningful values of entropy changes from relaxation measurements. Table 1 lists ten motional models that we have considered in evaluating the relation between conformational entropy, S_p, and S^2_{LZ}. Several of the models that have been chosen are commonly used in the interpretation of NMR relaxation data in terms of motional parameters. These models provide a simple physical interpretation of the molecular dynamics. Some of the other models that have been considered do not provide a straightforward physical picture and are intended only to investigate how sensitive the S_p *versus* S^2_{LZ} profile is to the mathematical form of the particular model. For simplicity we describe the models by giving the probability density, $p(\theta, \phi)$. Once $p(\theta, \phi)$ is known it is possible to evaluate conformational entropy, S_p, directly from equation (16).

The first two models in Table 1 are discussed in detail in Methods and describe motion of a bond vector on the surface of a cone of angle θ_0. In the first model motion is governed by a harmonic potential, while the second model assumes that the probability of each value of ϕ, for $0 \leqslant \phi \leqslant \phi_0$, is equal and non-zero. Model 1 is related to the

Table 1. Probability density functions used to calculate S_p *versus* S^2_{LZ} profiles

Model	Probability density function, $p(q)$
1	$\exp(-\eta\phi^2/2)/\int_0^{2\pi}\exp(-\eta\phi^2/2)d\phi$, $\theta=\theta_0$; 0 for $\theta\neq\theta_0$
2	$1/(\phi_0)$ for $0\leqslant\phi\leqslant\phi_0$, $\theta=\theta_0$; 0 for $\phi>\phi_0$ or $\theta\neq\theta_0$
3	$1/\{\phi_0(1-\cos\theta_0)\}$ for $0\leqslant\theta\leqslant\theta_0$ and $0\leqslant\phi\leqslant\phi_0$; 0 for $\theta>\theta_0$ or $\phi>\phi_0$
4	$1/\int_0^{2\pi}\int_0^{\theta_B(\phi)}\sin\theta\ d\theta\ d\phi$, where $\theta_B(\phi)=(\cos^2\phi/\theta_S^2+\sin^2\phi/\theta_L^2)^{-1/2}$
5	$(1/2\pi)\exp(-\eta\theta^2)/\int_0^{\pi}\exp(-\eta\theta^2)\sin\theta\ d\theta$
6	$(1/2\pi)\exp(-\eta\sin^2\theta)/\int_0^{\pi}\exp(-\eta\sin^2\theta)\sin\theta\ d\theta$
7	$(1/2\pi)\exp(-\eta\theta^4)/\int_0^{\pi}\exp(-\eta\theta^4)\sin\theta\ d\theta$
8	$(1/2\pi)\exp(-\eta\sin\theta)/\int_0^{\pi}\exp(-\eta\sin\theta)\sin\theta\ d\theta$
9	$(1/2\pi)(1+\eta\theta^6)^{-1}/\int_0^{\pi}(1+\eta\theta^6)^{-1}\sin\theta\ d\theta$
10	$(1+\eta_1\theta^6+\eta_2\phi^6)^{-1}/\int_0^{2\pi}\int_0^{\pi}(1+\eta_1\theta^6+\eta_2\phi^6)^{-1}\sin\theta\ d\theta\ d\phi$

Gaussian axial fluctuation model suggested by Bruschweiler & Wright (1994). Note that for each value of the force constant η (model 1) or ϕ_0 (model 2) there are unique values of S_p and S^2_{LZ}. The model most widely used to describe internal motion is diffusion-in-a-cone (Brainard and Szabo, 1981: model 3 in Table 1). Typically in this case, it is assumed that the bond vector in question diffuses freely in the angular region $0\leqslant\theta\leqslant\theta_0$, $0\leqslant\phi\leqslant2\pi$. We have extended this model somewhat by considering the case of free diffusion within the boundary $0\leqslant\theta\leqslant\theta_0$, $0\leqslant\phi\leqslant\phi_0$. For this particular model, as for the first two examined, it is possible to provide an analytical solution. The values of S^2_{LZ} and S_p (model 3) are given by:

$$S_p/k=\ln\{\phi_0(1-\cos\theta_0)\} \tag{21.1}$$

and

$$\begin{aligned}S^2_{LZ}=&\cos^2\theta_0(1+\cos\theta_0)^2/4+2/3\\&\sin^6\theta_0(1-\cos\phi_0)/\{(1-\cos\theta_0)^2\phi_0^2\}+3/8\\&(\cos\theta_0-(1/3)\cos^3\theta_0-2/3)^2(1-\cos2\phi_0)/\\&\{(1-\cos\theta_0)^2\phi_0^2\}\end{aligned} \tag{21.2}$$

Yamasaki *et al*. (1995) have analyzed the dynamics of the backbone N-H^N bond vectors of RNase HI using a 420 ps molecular dynamics trajectory of the protein. The authors note that the distribution of the majority of the backbone N-H^N bond vectors can be approximated by the diffusion-in-a-cone model. However, the distributions were, in general, elliptic, with the long axis of the ellipse perpendicular to the plane defined by the N-H^N and N-C^α bond vectors. Model 4 provides a description of such a trajectory, where θ_S and θ_L are the minimum and maximum semi-angles that the bond vector makes on the surface of the cone, respectively. We show below that models 3 and 4 give very similar S^2_{LZ} *versus* S_p profiles for values of θ_S and θ_L typically observed in molecular dynamics trajectories ($\theta_L/\theta_S\sim2$).

Models 5 to 9 describe motions of bond vectors that are axially symmetric. Model 5 is similar to the diffusion-in-a-cone model with $\phi_0=2\pi$, except that the distribution of bond vectors about the symmetry axis is Gaussian. The next example, model 6, describes the case where there are two distributions of bond vector motions, centered at $\theta=0$ and π. This gives rise to a ''double-cone'' type of motion, which has been observed in a number of molecular dynamics trajectories (Yamasaki *et al*., 1995) and used to interpret ^{15}N relaxation data for the protein, interleukin-1β (Clore *et al*., 1990). Models 7 to 9 are included to allow an assessment of how different forms for axially symmetric probability densities affect estimate of S_p from S^2_{LZ} values. Finally, a simple example of a non-axial probability distribution is considered in model 10 and will be discussed later.

Figure 1 illustrates the relation between S_p and S^2_{LZ} for a number of the models considered in Table 1 (model 3 with $\phi_0=2\pi$ and models 5 to 9). Note that for values of S^2_{LZ} extending from about 0.1 to 0.7 the entropy decreases with increasing S^2_{LZ} in a linear fashion ($dS_p/dS^2_{LZ}\sim-2.7$ k). As the value of S^2_{LZ} increases from $\sim$0.7 there is a rapid decrease in S_p. Recall from the discussion above that for values of S^2_{LZ} greater than $\sim$0.95 the classical approach breaks down and therefore the results of Figure 1 are no longer valid. While the profiles associated with these different models (i.e. model 3 with $\phi_0=2\pi$ and models 5 to 9) are clearly distinct, it is important to note that for a given change in order parameter, the change in conformation entropy is relatively independent of the model considered. This is illustrated in Table 2 (column 2),

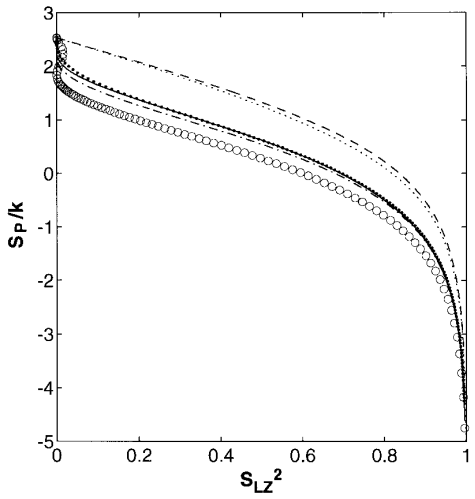

Figure 1. Conformational entropy, S_p (classical derivation) *versus* S^2_{LZ} for (○) model 3 ($\phi_0=2\pi$), model 5 (●●●●), model 6 (– – – –), model 7 (– · – · –), model 8 (· · · ·) and model 9 (——).

Table 2. Conformational entropy changes associated with ps-ns timescale bond vector fluctuations for defined changes in order parameters

ΔS^2_{LZ} ($S^2_{LZ,b} - S^2_{LZ,a}$)	Average ΔS_p (models 3 – 9) (J / mol K)[a]	ΔS_p (eqn 24) (J / mol K)	Average ΔS_p (models 1,2) (J / mol K)	ΔS_p (model 10) (J / mol K)
0.05 – 0.95	31.99 ± 1.74	30.50	19.13 ± 0.44	45.70
0.10 – 0.90	24.11 ± 0.74	23.15	14.91 ± 0.24	33.66
0.15 – 0.85	19.20 ± 0.46	18.46	12.26 ± 0.00	26.30
0.20 – 0.80	15.49 ± 0.56	14.85	9.67 ± 0.31	21.23
0.25 – 0.75	12.44 ± 0.46	11.82	7.66 ± 0.27	16.40
0.30 – 0.70	9.56 ± 0.29	9.15	5.97 ± 0.32	12.67
0.35 – 0.65	6.98 ± 0.30	6.70	4.24 ± 0.08	9.27
0.40 – 0.60	4.54 ± 0.27	4.39	2.91 ± 0.08	6.15
0.45 – 0.55	2.22 ± 0.17	2.18	1.49 ± 0.17	3.06

[a] In model 3 two cases were considered: $\phi_0 = 2\pi$ and $\phi_0 / \theta_0 = 2$; model 4, $\theta_L / \theta_S = 2$; model 10 $\eta_1 / \eta_2 = 1$.

where for a given change in the value of S^2_{LZ} the average value of ΔS_p and the standard deviation of ΔS_p is given for models 3 to 9 (model 3, for $\phi_0 = 2\pi$ and for $\phi_0 / \theta_0 = 2$; model 4, $\theta_L / \theta_S = 2$). While models 3 to 9 given similar values of ΔS_p, Table 2 shows that models 1 and 2 give significantly lower values, while model 10 predicts a much larger change in ΔS_p for a given change in order parameter. Thus, Table 2 indicates that, in general, values of ΔS_p can be very much dependent on the model used to describe the bond vector motion. This is discussed more fully below.

In the case of diffusion-in-a-cone (model 3) with $\phi_0 = 2\pi$, it is of interest to note that for $S^2_{LZ} \leqslant 1/64$ there is not a 1:1 correspondence between entropy and order parameter. In fact, for $S^2_{LZ} < 1/64$ there are three values of S_p that are possible for every value of the order parameter. For this model an analytical expression connecting S_p and S^2_{LZ} can be derived from equation (21) and is given by:

$$S_p / k = \ln \pi[3 - (1 + 8S_{LZ})^{1/2}], \; 0 \leqslant S^2_{LZ} \leqslant 1$$

$$S_p / k = \ln \pi[3 \pm (1 - 8S_{LZ})^{1/2}], \; 0 \leqslant S^2_{LZ} \leqslant 1/64 \quad (22)$$

Although it is not possible to derive equations relating S_p and S^2_{LZ} for the majority of models considered in Figure 1, an approximate relation:

$$S_p / k = A + \ln \pi[3 - (1 + 8S_{LZ})^{1/2}] \qquad (23)$$

where A is a model-dependent constant fits these profiles remarkably well. This is illustrated for a number of the models in Figure 2. That a single model is able to fit the data so well is perhaps not surprising, considering that (1) each of models 3 to 9 describes motion within a solid volume and (2) each of models 5 to 9 depend only on a single parameter (η) with the same holding true for models 3 and 4, provided that the value of ϕ_0 (model 3) and the ratio of θ_L / θ_S (model 4) are fixed. In contrast, models 1 and 2 describe motion on a surface and it is clear from inspection of Table 2 that for a given ΔS^2_{LZ} there will be significant differences in ΔS_p depending on whether the model employed is one that describes motion within a solid volume or on a surface. Not surprisingly, the model that confines the motion to the surface predicts smaller entropy changes.

Note that the entropy-order parameter profiles of all models considered to this point depend on only a single parameter (e.g. η in models 1 and 5 to 9; ϕ_0 in model 2; θ_0 in model 3 with $\phi_0 = 2\pi$). In order to evaluate how the entropy *versus* order parameter profile changes with increasing complexity of the model employed, consider diffusion-in-a-cone with $0 \leqslant \theta \leqslant \theta_0$, $0 \leqslant \phi \leqslant \phi_0$, $\theta_0 / \phi_0 \leqslant 1$ (i.e. $0 < \theta_0 \leqslant \pi$ and $\theta_0 \leqslant \phi_0 \leqslant 2\pi$). This is a special case of model 3, but unlike previous discussions of model 3, the condition $\phi_0 = 2\pi$ is now relaxed. For each randomly selected value of θ_0 within the range of $0 < \theta_0 \leqslant \pi$, a value of ϕ_0 satisfying $\theta_0 \leqslant \phi_0 \leqslant 2\pi$ is chosen. For each (θ_0, ϕ_0) pair, a probability density $p(\theta, \phi) = 1 / \{\phi_0(1 - \cos\theta_0)\}$, $0 \leqslant \theta \leqslant \theta_0$, $0 \leqslant \phi \leqslant \phi_0$ is obtained, from which the values S_p and S^2_{LZ} are calculated in the manner described in detail above. A plot of S_p *versus* S^2_{LZ} obtained from 2000 (θ_0, ϕ_0)

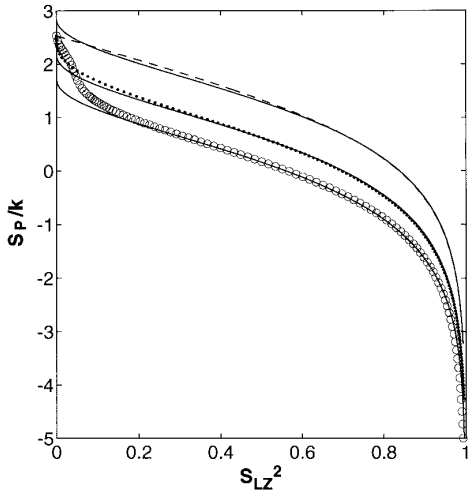

Figure 2. Conformational entropy, S_p (classical derivation) *versus* S^2_{LZ} for (○) model 3 ($\theta_0 / \phi_0 = 0.5$), model 5 (●●●●) and model 6 (– – – –). Each profile is fit to equation (23) and the best fit is indicated with the continuous line. Values of A are –0.11, 0.34 and 1.02 for models 3, 5 and 6, respectively; see equation (23).

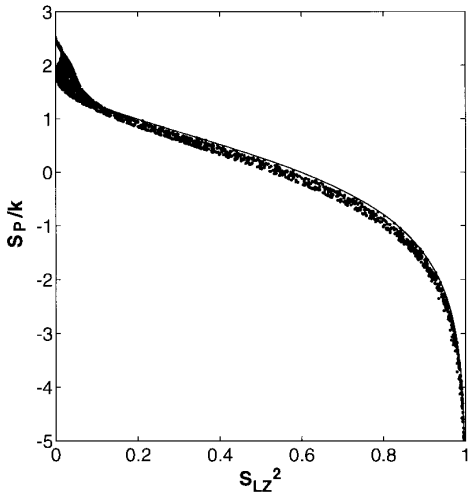

Figure 3. Conformational entropy, S_p *versus* S^2_{LZ} using the diffusion in a cone model (model 3 Table 1) with a probability density $p(\theta, \phi)$ given by $p(\theta, \phi) = 1/\{(1 - \cos\theta_0)\phi_0\}$, $\theta_0/\phi_0 \leqslant 1$. S_p was calculated using the approach based on classical statistics described in the text with 2000 (θ_0, ϕ_0) values chosen randomly. For comparison, the case of $\phi_0 = 2\pi$ is plotted with the continuous line.

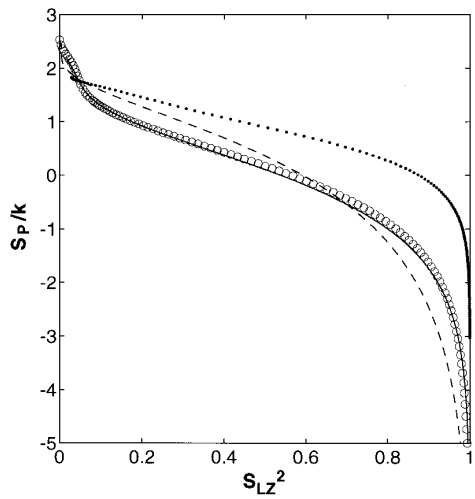

Figure 4. Conformational entropy, S_p (derived classically) *versus* S^2_{LZ} illustrating the differences in ΔS_p that are predicted for a given change in order parameter using a number of different models. Models 1 (●●●●), 3 (○, $\theta_0/\phi_0 = 0.5$), 4 (——, $\theta_L/\theta_S = 2$) and 10 (– – – –, $\eta_1/\eta_2 = 1$) are considered.

pairs is illustrated in Figure 3. For comparison, the case of $\phi_0 = 2\pi$ is considered and is indicated by the continuous line in the Figure. Note that there is no longer a 1:1 correspondence between S_p and S^2_{LZ} for any value of the order parameter. Additional simulations have shown that when the restriction $\theta_0/\phi_0 \leqslant 1$ is relaxed, the spread in entropy values associated with a given order parameter increases significantly. Clearly, in these cases a given change in order parameter cannot be interpreted in terms of a defined change in conformational entropy.

Figure 4 illustrates further the difficulties associated with relating entropy changes to order parameter changes when the model describing the motion of the bond vector in question is not known. A number of different models are shown, selected from the examples illustrated in Table 1 to articulate this point. It is clear that as the motion becomes less restricted there is a corresponding greater entropy change associated with a particular change in order parameter. For example, for model 1, which describes oscillatory motion on the surface of a cone, a change in S^2_{LZ} from 0.8 to 0.2 corresponds to ΔS_p of 10 J/mol K, while model 3 with $\phi_0 = 2\pi$ gives $\Delta S_p = 15$ J/mol K. In contrast, model 10 with $\eta 1/\eta 2 = 1$, predicts that for the same change in the order parameter, $\Delta S_p = 21$ J/mol K. These results, summarized in Table 2, strongly suggest the importance of understanding bond vector motion prior to correlating changes in NMR-derived motional parameters with changes in thermodynamic parameters, such as conformational entropy.

Insight into motions of bond vectors in complex macromolecules such as proteins can be obtained from molecular dynamics simulations and a significant number of such investigations have appeared in the literature (Philippopoulos & Lim, 1995; Yamasaki *et al*., 1995; Chandrashekhar *et al*., 1992; Smith *et al*., 1995; Palmer & Case, 1992). Here, we have made use of a 1.12 ns molecular dynamics trajectory of fully solvated *E. coli* ribonuclease HI (RNase HI) kindly provided by C. Lim and M. Philippopoulos, to address whether any of the models considered above are suitable to describe bond vector dynamics that occur in proteins. (Note that in the original paper (Philippopoulos & Lim, 1995) a 500 ps trajectory was reported; since the time of publication of this work the simulation has been extended to 1.12 ns.) Values of S^2_{LZ} and S_p were calculated from a 1.12 ns trajectory using only the final 800 ps, as described in detail in Methods. In the analysis we have included backbone N-H^N and C^α-H^α bond vectors as well as all side-chain N-H^N bond vectors whose correlation functions converge during the course of the trajectory (see Methods). Remarkably, the S_p *versus* S^2_{LZ} profile is well fit by equation (23) with $A = 0$ (Figure 5); that is, given the limitations of the RNase HI molecular dynamics simulation considered here (see below), the data suggest that the diffusion-in-a-cone model (with $\phi_0 = 2\pi$) can be used to estimate conformational entropy changes from changes in order parameters for both backbone N-H^N and C^α-H^α and side-chain N-H^N bond vectors. This statement is not meant to imply that the motion of the bond vectors in RNase HI is accurately described by model 3. Although we do find that for the majority of cases the (θ, ϕ) bond vector distribution is reasonably approximated by the cone model, the distribution is not at all uniform.

It must be emphasized that only a single protein dynamics simulation has been considered and that the trajectory of only 800 ps was included in the

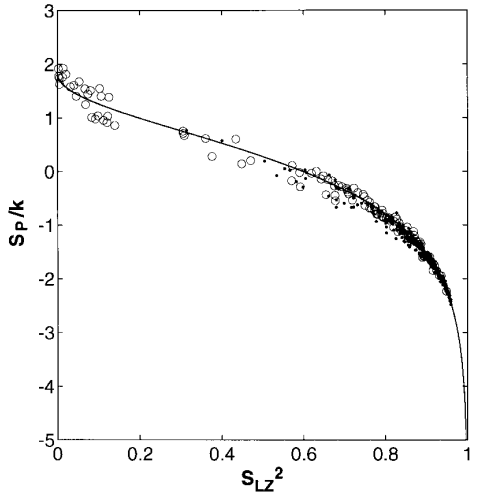

Figure 5. Conformational entropy, S_p *versus* S^2_{LZ} calculated from the final 800 ps of a molecular dynamics trajectory of the (hydrated) protein RNase HI (Philippopoulos & Lim, 1995). Backbone N-H^N and C^α-H^α(·), and side-chain N-H^N bond vectors (○) are included.

above analysis. NMR relaxation experiments are sensitive to motions with frequencies on the order of the inverse of the molecular correlation time or faster (Lipari & Szabo, 1982a, b), although in some cases information can be extracted about much slower processes through a field-dependent T_2 study or a set of $T_{1\rho}$ experiments (Deverell *et al*., 1970; Szyperski *et al*., 1993; Akke & Palmer, 1996). Thus, a 1.12 ns trajectory is clearly of insufficient length to completely sample the range of conformations that would be reported on by NMR relaxation experiments. Nonetheless, the results illustrated in Figure 5, though incomplete, are extremely encouraging. The development of faster computers and more efficient computational algorithms will facilitate the recording of longer dynamics trajectories, leading to significant improvements in our understanding of molecular dynamics. In the absence of such data at present, however, we propose to approximate the contribution to the change in conformational entropy associated with the transition from state a to state b, and arising from changes in ps-ns timescale bond vector fluctuations in the two states, by using the cone-model. For this case:

$$\Delta S_p(j)/k = \ln\{[3 - (1 + 8S_{\mathrm{LZ,b}})^{1/2}]/ [3 - (1 + 8S_{\mathrm{LZ,a}})^{1/2}]\} \quad (24)$$

where $S_{\mathrm{LZ,a}}$ and $S_{\mathrm{LZ,b}}$ are the order parameters of the bond in states a and b, respectively. Assuming that there is no change in kinetic energy from state a to state b, it follows that $\Delta S_p(j) = \Delta S(j)$, where $\Delta S(j)$ is the total rotational entropy change for bond j, which includes both kinetic and potential energy contributions (see equation (12)).

Equation (24) can be used to estimate conformational entropy changes associated with a change from state a to state b, providing that NMR relaxation data are available on the macromolecule in both states. The change may be the result of the binding of a ligand to a macromolecule or the binding of one macromolecule to another. The methodology provided here and by Akke *et al*. (1993), links NMR-derived motional parameters with thermodynamics quantities, allowing extraction of thermodynamic values on a per-residue basis. This type of residue-specific information cannot be obtained with other non-NMR-based experimental approaches.

As described in Theory, a number of important assumptions are involved in any attempt to relate NMR-derived dynamics parameters with contributions to conformational entropy associated with ps-ns timescale bond-vector dynamics. Specifically, we have assumed that the partition function describing the molecular system can be factored into two independent contributions arising from NMR-observable and NMR-unobservable motions. In the event of a correlation between such motions, the entropy calculated from the equations derived herein will represent an upper estimate (Akke *et al*., 1993). Some insight into the ''interplay'' between dynamics occurring on different timescales can be obtained by examination of a number of NMR relaxation studies. Stone *et al*. (1992) studied the backbone dynamics of the glucose permease IIA domain by ^{15}N relaxation methods and concluded that there was no relation between the calculated R_{ex} values, which are indicative of motions on the μs-ms timescale and either τ_e values or the measured amide proton exchange rates. Note that τ_e values are sensitive to ps-ns motions, while amide exchange measures dynamics on ms or longer timescales. Kordel *et al*. (1992) noted three distinct categories of correlation between backbone order parameters (reporting on ps-ns dynamics) and amide hydrogen exchange rates for the case of calcium-loaded calbindin D_{9k}. Some residues displayed slow solvent exchange and high order parameters, some showed rapid exchange with solvent and low order parameters, while yet another category with rapid solvent exchange and high order parameters exists. Thus, the data indicate that there need not be a correlation between high flexibility on the ps-ns time scale and a high propensity for flexibility in the ms time regime. Kay *et al*., (1996) compared the ps-ns dynamics at the interface of an SH2-phosphopeptide complex with the lineshapes of crosspeaks in the complex (Pascal *et al*., 1995). Notably, broadening of the aliphatic resonances of the four Arg residues in the phosphotyrosine binding region was observed, due to the modulation of their chemical shifts by μs-ms timescale motion. Broadening is not observed in any other region of the binding interface. In contrast, there was no indication for above-average ps-ns motions at the phosphotyrosine site, while other regions of the binding site (the hydrophobic binding region) showed high levels of ps-ns dynamics. Thus, the data indicate no evidence for correlation between

high (ns-ps) and low-frequency (μs-ms) motions in this molecular complex. The examples provided above do not, in any way, prove the validity of equation (4). Nevertheless, they suggest that the assumption regarding the separation of NMR-observable motions (ps-ns), which contribute to rotational entropy (and can be measured by spin relaxation), from significantly slower processes is at least a reasonable first-order approximation.

An additional assumption that we and others (Akke *et al*., 1993) have made is that each fluctuating bond vector is independent of all others. Analysis of a 1.12 ns trajectory of RNase HI indicates that the ps timescale motions of backbone N-H^N bond vectors in well-structured regions of the molecule are essentially independent. In contrast, motions of bond vectors within a given side-chain can show high levels of correlation, although the extent varies significantly both for different bonds within a given residue and for different residues. It is therefore not possible to generalize regarding the accuracy of equation (5). However, it is possible to state that in all cases the simplifications may result in an overestimate in calculated thermodynamic parameters.

As an example of the utility of the methods developed, we consider an application measuring the contributions from rapid bond vector motions to the conformational entropy change associated with a folding transition involving the N-terminal SH3 domain of the *Drosophila* signal transduction protein drk (drkN SH3). This protein has been characterized in detail and shown to exist in equilibrium between a folded and an unfolded form in aqueous buffer and near neutral pH (Zhang & Forman-Kay, 1995). We have recently measured ^{15}N T_1, T_2 relaxation times and steady-state ^1H-^{15}N NOE values for a system consisting of folded and unfolded forms of the protein in equilibrium (Farrow *et al*., 1995). Values of the spectral density function of the backbone amide bond vectors for 11 well-resolved residues have been established at a number of frequencies. In addition, a Lipari-Szabo analysis of the data has been performed. Table 3 lists the residues that were included in this analysis, the values of S^2_{LZ} in both the folded and unfolded states, and the conformation entropy change on a per-residue basis associated with the folding-unfolding transition obtained using equation (24). It is important to recognize that because NMR relaxation experiments are sensitive to motions on the ps-ns timescale, the changes in entropy calculated in Table 3 reflect only changes in the rapid motions visible by NMR. Of course, additional contributions from slower motional processes, other bond vectors and solvent will be involved in the net entropy change. In this regard, it is of interest to note that the magnitude of the entropy change that is observed (average entropy change per residue of 12 J/mol K) is similar to the average entropy change per residue that has been estimated for protein folding from a number of different techniques (Doog and Sternberg, 1995), ~14 J/mol K. In the Lipari-Szabo analysis of the relaxation data it is assumed that a single correlation time can describe the overall rotation of the unfolded state. Clearly, this is an over simplification and indeed a mean value of τ_m = 5.8 ns with a standard deviation of 1.5 ns was obtained for the 11 residues considered in the unfolded drkN SH3 domain (Farrow *et al*., 1995). If optimum τ_m and S^2_{LZ} values are calculated on a per residue basis (i.e. if a separate τ_m value is allowed for each residue in the unfolded state), the average entropy change per residue increases by approximately 10% relative to the value obtained under the assumption of a single global correlation time. With the exception of Ile 48, for which ΔS_p increases by a factor of 1.5, changes in ΔS_p are within 10% when calculated using the two different methods. While a precise quantification of entropy changes at a given site is difficult in the absence of a proper model describing the dynamics of unfolded protein states, the result obtained nevertheless suggest that entropy changes, like changes in free energy, are comprised of a large number of compensating terms and that rapid time scale bond vector fluctuations can contribute significantly to thermodynamic parameters (Akke *et al*., 1993).

Table 3. Contributions to the conformational entropy change associated with the folding-unfolding transistion of the N-terminal SH3 domain of drk (Zhang & Forman-Kay, 1995) from ps-ns timescale fluctuations of N-H^N bond vectors

Residue	S^2_{LZ} (folded)	S^2_{LZ} (unfolded)	ΔS_p (J/mol K)
Ala 3	0.86 ± 0.01	0.28 ± 0.06	16.5 ± 1.3
Thr 12	0.77 ± 0.01	0.25 ± 0.05	12.6 ± 1.1
Ala 13	0.77 ± 0.02	0.26 ± 0.10	12.4 ± 2.1
Asp 14	0.83 ± 0.01	0.56 ± 0.10	9.0 ± 2.4
Thr 22	0.93 ± 0.01	0.79 ± 0.02	9.6 ± 1.5
Trp 36	0.91 ± 0.02	0.57 ± 0.07	14.3 ± 2.5
Trp 36'	0.82 ± 0.02	0.34 ± 0.09	13.1 ± 2.0
Arg 38	0.85 ± 0.02	0.72 ± 0.04	5.7 ± 1.8
Gly 43	0.81 ± 0.01	0.54 ± 0.12	8.5 ± 2.8
Gly 46	0.87 ± 0.01	0.19 ± 0.09	18.9 ± 2.0
Ile 48	0.86 ± 0.01	0.55 ± 0.02	10.9 ± 0.8
Ser 50	0.90 ± 0.02	0.54 ± 0.02	14.1 ± 1.8

$\Delta S_p = S_p$(unfolded) – S_p(folded). Data from the indole N-H^N of Trp36 are indicated by Trp36'. Values are calculated from equation (24).

Concluding Remarks

In this study, relations between conformational entropy and NMR-derived order parameters have been established for several models of bond vector motion. It has been shown in the case of a number of simple models that classical and quantum mechanical approaches give very similar S_p *versus* S^2_{LZ} profiles, so long as $S^2_{LZ} \leqslant 0.95$. As the complexity of the motion increases, the absolute entropy change associated with a given change in order parameter becomes larger. Thus, the diffusion-on-a-cone model predicts a smaller change in entropy than diffusion-in-a-cone, for a defined change in order parameter. A 1.12 ns molecular dynamics

trajectory of fully hydrated RNase HI has been analyzed and an entropy-order parameter profile generated for backbone N-H^N and C^α-H^α, and side-chain N-H^N bond vectors. Remarkably, the profile obtained can be fit using the diffusion-in-a-cone model. This allows a simple analytical expression to be employed relating, on a per-residue basis, changes in order parameter with changes in entropy associated with ps-ns timescale dynamics.

Methods

Calculation of the relation between S^2_{LZ} and S_p from a molecular dynamics trajectory

The final 800 ps (0.32 to 1.12 ns) of a 1.12 ns RNase HI trajectory (Philippopoulos & Lim, 1995) was divided into 4000 steps each of 0.2 ps and the effects of overall rotation removed by a least-squares fitting of backbone C^α atoms of each of the 4000 structures to the backbone C^α atoms of the average structure generated by averaging coordinates for each of the 4000 steps. For each of the bond vectors, $\mathbf{r}_i$, a new z axis direction is given by $\Sigma_l \mathbf{r}_i(l)$, where the sum extends over all 4000 steps (l = 1, 4000) of the trajectory. The coordinates of each bond vector are transformed into this new frame. Note that for each X-H^X bond vector, (X = N or C), the coordinate frame is centered on the X atom. For each bond vector, (θ, ϕ) values are calculated for each of the 4000 steps according to the relation $\theta = \cos^{-1}(z/r)$, $x = r\sin\theta\cos\phi$, $y = r\sin\theta\sin\phi$ and $r = (x^2 + y^2 + z^2)^{0.5}$. In this frame, θ extends from 0 to some maximum value, θ_{max}. The probability density $p(\theta, \phi)$ was calculated by dividing the trajectory along θ into 90 equal steps, so that $\theta_i = [(i-1)\Delta\theta + i\Delta\theta]/2 = i\Delta\theta - \Delta\theta/2$, $\Delta\theta = \theta_{max}/90$. In order to account for the fact that as θ_i becomes larger it is increasingly important to parse ϕ into smaller steps, we used the following approach. For a given θ_i, ϕ_i is divided into M_i steps each of size $2\pi/M_i$, where $M_i = \mathrm{INT}\{\sin(\theta_i)/\sin(\Delta\theta)\}$ (i.e. the first step extends from $0 \leqslant \phi_i < 2\pi/M_i$, the second from $2\pi/M_i \leqslant \phi_i < 4\pi/M_i$, etc.). The value of ϕ_i in each of the M_i steps is given by $\phi_{i,j} = [(j-1)2\pi/M_i + j2\pi/M_i]/2 = j2\pi/M_i - \pi/M_i (1 \leqslant j \leqslant M_i)$. The number of times that a given bond vector lies within a surface extending from $(i-1)\Delta\theta$ to $(i)\Delta\theta$ and from $(j-1)2\pi/M_i \leqslant \phi < 2\pi j/M_i$ is counted and divided by $4000\sin(\theta_i)\Delta\theta_i(2\pi/M_i)$ to give $p(\theta_i,\phi_{ij})$. Note that the factor of 4000 takes into account the number of steps in the trajectory. The values of S_p and S^2_{LZ} are obtained by the summations:

$$S_p/k = -\Sigma_{i=1,90}\Sigma_{j=1,M_i} [p(\theta_i,\phi_{i,j})\ln\{p(\theta_i,\phi_{i,j})\}\sin(\theta_i)\Delta\theta_i(2\pi/M_i)]$$

and

$$S^2_{LZ} = (4\pi/5)\Sigma_{r=-2,2}|\Sigma_{i=1,90}\Sigma_{j=1,M_i} [Y_{2r}(\theta_i,\phi_{i,j})p(\theta_i,\phi_{i,j})\sin(\theta_i)\Delta\theta_i(2\pi/M_i)]|^2$$

The value of S^2_{LZ} was also obtained from equation (19) and the maximum difference in calculated S^2_{LZ} between the two methods is less than 0.004. Only the bond vectors whose trajectories had converged were included in the calculations. We found empirically that the following computational approach worked well for removing bond vectors with trajectories that had not converged. (1) The normalized scalar product $\alpha(t) = \{\mathbf{r}_i(t)\mathbf{r}_i(0)\}/\{|\mathbf{r}_i(t)||\mathbf{r}_i(0)|\}$ was calculated for each of the 4000 time-points, t and $\alpha(t)$ divided into 40 equal time periods (period 1 extending for the first 100 time-points, period 2 the next 100, etc.). The value of $\alpha(t)$ was averaged over the 4000 time-points to give α_{avg} and averaged over each of the 40 time periods to give $\alpha_{avg}(k)$. The maximum and minimum values of $\alpha_{avg}(k)\{k = 1,40\}$, α_{max} and α_{min}, were selected. If $|(\alpha_{max} + \alpha_{min})/2 - \alpha_{avg}| > 0.3$ then the bond vector was excluded. (2) The value of $\alpha(t)$ was calculated and $\alpha(t)$ divided into three equal time periods. The values of $\alpha(t)$ were averaged in each of the three intervals. If the difference between the maximum and minimum of the averaged values was larger than 0.55, the bond vector was excluded. Using criteria (1) and (2), three of the 149 backbone N-H^N vectors, two of the 169 C^α-H^α vectors and 27 of the 139 side-chain N-H^N vectors were excluded from the analysis. The N-terminal amino group was not considered.

Derivation of equation (12)

From equation (11) and $A = -kT \ln z(j)$ we can immediately write:

$$-A = kT\ln\{f(T)\} + kT\ln\{\textstyle\int_v \exp\{-U(q)/(kT)\}\mathrm{d}v\} \quad (25)$$

The contribution from each term on the right-hand side of equation (25) to the entropy can be evaluated using equation (1). The first term on the right-hand site of equation (25) gives:

$$S_1 = k[T\mathrm{d}\{\ln f(T)\}/\mathrm{d}T + \ln\{f(T)\}] \quad (26)$$

while the second term contributes

$$S_2 = k\ln[\textstyle\int_v \exp\{-U(q)/(kT)\}\mathrm{d}v] + kT\partial[\ln(\int_v \exp\{-U(q)/(kT)\}\mathrm{d}v)]/\partial T \quad (27)$$

We note that:

$$\begin{aligned} &k\ln[\textstyle\int_v \exp\{-U(q)/(kT)\}\mathrm{d}v] \\ &= k\textstyle\int_{v'} P\mathrm{d}v'[\ln(\int_v \exp\{-U(q)/(kT)\}\mathrm{d}v)] \\ &= k\textstyle\int_{v'} P(\ln(\int_v \exp\{-U(q)/(kT)\}\mathrm{d}v)]\mathrm{d}v' \end{aligned} \quad (28)$$

where P is the probability density given by equation (13), and:

$$\textstyle\int_{v'} P\mathrm{d}v' = 1 \quad (29)$$

In addition, we can write:

$$\begin{aligned} kT\partial[\ln(\textstyle\int_v \exp\{-U(q)/(kT)\}\mathrm{d}v)]\partial T &= (1/T)\textstyle\int_v PU(q)\mathrm{d}v \\ &= -k\textstyle\int_v P\ln[\exp\{-U(q)/(kT)\}]\mathrm{d}v \end{aligned} \quad (30)$$

Therefore:

$$\begin{aligned} S_2 &= k\textstyle\int_{v'} P[\ln(\int_v \exp\{-U(q)/(kT)\}\mathrm{d}v)]\mathrm{d}v' \\ &\quad -k\textstyle\int_v P\ln[\exp\{-U(q)/(kT)\}]\mathrm{d}v \\ &= -k\textstyle\int_{v'} P\ln[\exp\{-U(q)/(kT)\}/(\int_v \exp\{-U(q)/ \\ &\quad \times (kT)\}\mathrm{d}v)]\mathrm{d}v' = -k\textstyle\int_{v'} P\ln\{P\}\mathrm{d}v' \end{aligned} \quad (31)$$

combining equations (26) and (31) gives:

$$S = S_1 + S_2 = k[T\mathrm{d}\{\ln f(T)\}/\mathrm{d}T + \ln\{f(T)\}] - k\textstyle\int_{v'} P\ln\{P\}\mathrm{d}v' \quad (32)$$

which is equation (12).

Calculation of S_p *versus* S^2_{LZ} profiles using both classical and quantum mechanical derivations

As a means of illustrating the differences (and similarities) between the classical and quantum mechan-

ical approaches as well as establish where the classical treatment becomes invalid, we derive the entropy-order parameter relation for a backbone N-H^N bond vector in a protein undergoing one-dimensional restricted rotation about the N-C^α bond axis. In the following we take the N-C^α bond vector as the *z*-axis and use a coordinate system centered on the N atom. Note that the motion of the N-H^N bond vector in this particular case can simply be described as diffusion on the surface of a cone with an angle of $\theta_0 = 118°$ with respect to the cone symmetry axis, given by the N-C^α bond vector.

Example 1: Motion of the N-H^N vector in a potential of the form $U(\phi) = 1/2\eta\phi^2$, $-\pi \leqslant \phi \leqslant \pi$. The solution to the problem based on the classical treatment can be obtained by writing the energy of the system as:

$$E = p_\phi^2/(2I) + 1/2\eta\phi^2, \quad -\pi \leqslant \phi \leqslant \pi \tag{33}$$

where p_ϕ is the angular momentum of the backbone H^N, η is a force constant and I is the moment of inertia for the H^N particle that rotates about the *z*-axis (N-C^α bond) at an angle of θ_0 (118° for peptide geometry). We can write $p_\phi = I\mathrm{d}\phi/\mathrm{d}t$ and $I = m_H r_{NH}^2 \sin^2\theta_0$ where $\mathrm{d}/\mathrm{d}t$ is a time derivative, m_H is the mass of the H^N atom, r_{NH} is the length of the N-H^N bond vector and θ_0 is the angle that the bond vector makes with respect to the symmetry axis. Substitution of equation (33) into equation (10) gives:

$$z(j) = 1/h(2\pi IkT)^{0.5}\int_{-\pi}^{\pi} \exp\{-\eta\phi^2/(2kT)\}\mathrm{d}\phi \tag{34}$$

and providing that $\eta/kT > 0.5$ the limits of integration for the integral in equation (34) can be replaced by $(-\infty,\infty)$. Numerical simulations indicate that this substitution introduces an error of less than 3% ($\eta/kT > 0.5$). This yields the simple relation:

$$z(j) = (1/h)2\pi kT(I/\eta)^{0.5} \tag{35}$$

The entropy, $S(j)$, is readily calculated as:

$$S_{CL}(j)/k = 1 + \ln\{(1/h)2\pi kT(I/\eta)^{0.5}\} \tag{36}$$

from equation (1), (2) and (35), where the subscript CL denotes the fact that this is the expression derived for entropy from classical mechanics. The value of $S_p(j)$, see equation (16), is given by:

$$S_p(j)/k = 0.5 + 0.5\ln(2\pi kT/\eta) \tag{37}$$

The quantum mechanical derivation begins by considering the Hamiltonian, H:

$$H = -h^2/(8\pi^2 I)\mathrm{d}^2/\mathrm{d}\phi^2 + (1/2)\eta\phi^2 \tag{38}$$

which describes the system. If the boundary conditions are extended from $-\pi \leqslant \phi \leqslant \pi$ to $-\infty \leqslant \phi \leqslant \infty$, the Hamiltonian in equation (38) describes the well-known one-dimensional harmonic oscillator and the eigenvalues are (Levine, 1974):

$$E_m = h\nu_0(0.5 + m),\ m = 0,1,2,\ldots,\ \nu_0 = [1/(2\pi)](\eta/I)^{0.5} \tag{39}$$

The partition function is given by:

$$\Sigma_m \exp\{-E_m(j)/(kT)\} = \exp\{-h\nu_0/(2kT)\}/(1-\exp\{-h\nu_0/(kT)\}) \tag{40}$$

Numerical simulations show that for the case where $-\pi \leqslant \phi \leqslant \pi$, the first 21 energy states are well approximated by equation (39) if $(2\pi/h)(\eta I)^{0.5} \geqslant 4$. Moreover, in the limit that $(2\pi/h)(\eta I)^{0.5} \geqslant 4$ and $\eta/(kT) \geqslant 0.6$, consideration of only the first 21 terms in the summation of equation (40) results in an error of less than 4.5%. Therefore, if $(2\pi/h)(\eta I)^{0.5} \geqslant 4$ and $\eta/(kT) \geqslant 0.6$, the partition function can be calculated accurately from the eigenstates of H given by equation (39) even for the boundary conditions $-\pi \leqslant \phi \leqslant \pi$. The entropy, $S_{QM}(j)$, is calculated directly from equations (1), (2) and (40):

$$S_{QM}(j)/k = -\ln(1-\exp\{-h\nu_0/(kT)\}) + \{h\nu_0/(kT)\}/[\exp\{h\nu_0/(kT)\} - 1] \tag{41}$$

where the subscript QM is used to indicate that this result is obtained from the quantum mechanical derivation.

It is straightforward to derive the square of the order parameter, S_{LZ}^2, from equation (20) providing that the probability density, $p(\theta,\phi)$, describing the orientation of the N-H^N bond vector in a molecular coordinate system is known. The value of $p(\theta,\phi)$ is obtained by the substitution $U(q) = (1/2)\eta\phi^2$, $\mathrm{d}v = \mathrm{d}\phi$ in equation (13), from which it follows that:

$$p(\theta,\phi) = \exp\{-\eta\phi^2/(2kT)\}/\int_{-\pi}^{\pi}\exp\{-\eta\phi^2/(2kT)\}\mathrm{d}\phi, \quad \theta = \theta_0 \tag{42.1}$$

$$= (2\pi kT/\eta)^{0.5}\exp\{-\eta\phi^2/(2kT)\},\ \eta/(kT) > 0.5 \text{ and } \theta = \theta_0 \tag{42.2}$$

and:

$$p(\theta,\phi) = 0 \text{ for } \theta \neq \theta_0 \tag{42.3}$$

Substitution of equation (42.2) into equation (20) gives:

$$S_{LZ}^2 = 1 - 3\sin^2\theta_0\{\cos^2\theta_0[1-\exp(-1/a)] + 0.25\sin^2\theta_0[1-\exp(-4/a)]\} \tag{43}$$

where $a = \eta/kT$. Note that equation (43) has been evaluated using equation (42.2) for the probability density, which is strictly valid only for $a > 0.5$. However, numerical simulations show that equation (43) is a good approximation to the true value of S_{LZ}^2 even when a <0.5 (i.e. numerical simulations indicated that errors in S_{LZ}^2 are less than 0.02 using equations (42.2) rather than equation (42.1) for a <0.5).

The curves describing the relation between $[S_{QM}(j) - S_{CL}(j)]/k$ and S_{LZ}^2 for values of the moment of inertia, I, set to 1×10^{-46} kgm^2, 5×10^{-46} kgm^2 and 25×10^{-46} kgm^2 and $T = 300$ K are shown in Figure 6a. (Note that the value of I for a methyl group rotating about the methyl 3-fold axis is 0.53×10^{-46} kgm^2). It is clear that for $S_{LZ}^2 < 0.95$ the difference between the values of entropy calculated using either quantum or classical approaches is very small $\{[S_{QM} - S_{CL}]/k < 0.05\}$ and relatively independent of the value of I. For $S_{LZ}^2 = 0.95$, $[S_{QM} - S_{CL}]/S_{QM} = 0.05$ for $I = 1\times10^{-46}$ kgm^2 and decreases to 0.002 for $I = 25\times10^{-46}$ kgm^2. However, for well-ordered systems ($S_{LZ}^2 > 0.95$) the classical and quantum results diverge, especially for small values of I. This is due to the fact that the vibrational frequency of the harmonic oscillator is proportional to $I^{-0.5}$ and the spacing between energy states therefore increases with decreasing I (see equation (39)). As the value of I decreases, the energy states are no longer continuous (i.e. $E_m - E_{m-1} \geqslant kT$) and equation (10) is not valid. The correct value of the partition function, is of course, still given by equation (6).

Example 2: Motion of the N-H^N vector in a potential of the form $U(\phi) = 0$, $0 \leqslant \phi \leqslant \phi_0$ and $U(\phi) = \infty$, $\phi > \phi_0$.

The calculations are similar to those described above in the case of the harmonic oscillator and the details are therefore omitted. We note, however, that this problem is formally equivalent to the well-known particle in a box with the dimension of the box replaced by ϕ_0 and the moment of inertia, I, substituted for the mass of the

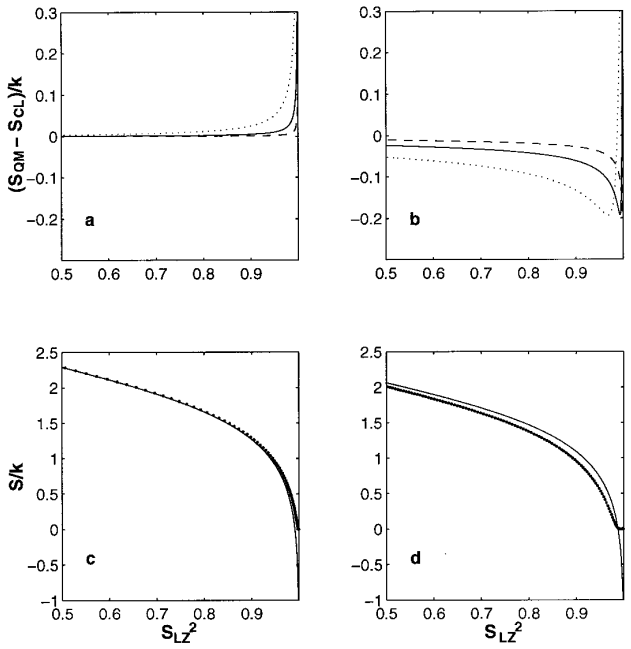

Figure 6. Comparison of the total entropy calculated using either a quantum mechanical approach (S_{QM}) or a classical approach (S_{CL}) as a function of order parameter squared, S^2_{LZ}. In a and b the difference between S_{QM} and S_{CL} is plotted, while in c and d the absolute values of S_{QM} and S_{CL} are indicated. A model of bond vector motion on the surface of a cone at an angle of 118° with respect to the cone symmetry axis is considered. A value of T = 300 K is used. In a and c a potential of the form $U(\phi) = 1/2\eta\phi^2$ is assumed, while in b and d free diffusion for $0 \leqslant \phi \leqslant \phi_0$ is considered. Values of I (moment of inertia) of 1×10^{-46} kgm^2 (· · ·), 5×10^{-46} kgm^2 (——) and 25×10^{-46} kgm^2 (– – – –) are included in a and b. In c and d a value of $I = 1 \times 10^{-46}$ kgm^2 is used and the results of the classical and quantum calculations are indicated by a continuous and dotted line, respectively. Note that the quantum results give S ⩾ 0 (see Methods).

particle (Levine, 1974). A straightforward calculation shows that the probability density is given by:

$$p(\theta, \phi) = 1/\phi_0, \ \theta = \theta_0, \ 0 \leqslant \phi \leqslant \phi_0$$
$$= 0, \ \theta \neq \theta_0 \ \text{or} \ \phi > \phi_0 \qquad (44)$$

where θ_0 is the angle between the N-H^N bond vector and the N-C$^\alpha$ axis (118°), as before. Calculating the entropy from classical mechanics gives:

$$S_{CL}(j)/k = 0.5 + \ln \phi_0 + \ln\{(1/h)(2\pi IkT)^{0.5}\} \qquad (45.1)$$

and:

$$S_p(j)/k = \ln\phi_0 \qquad (45.2)$$

A quantum mechanical solution is accomplished by noting that the eigenstates are given by (Levine, 1974):

$$E_m = -h^2m^2/(8I\phi_0^2), \ m = 1,2,3, \ldots \qquad (46)$$

with the partition function expressed as:

$$z(j) = \Sigma_m \exp\{-h^2m^2/(8IkT\phi_0^2)\} \qquad (47)$$

In equation (47) the sum extends from m = 1 to ∞. Note that the partition function and hence the entropy (equation (8)) must be calculated by evaluating the sum in equation (47) numerically.

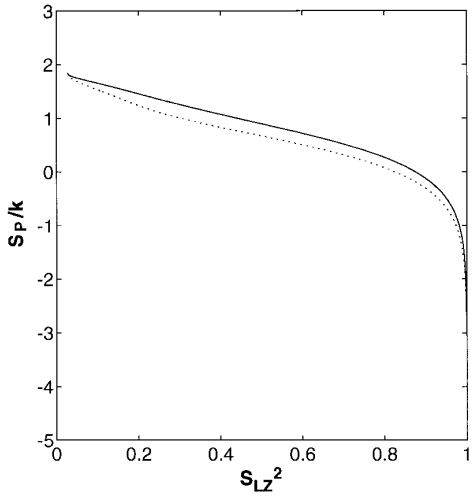

Figure 7. Conformational entropy, (S_p), derived classically, as a function of S^2_{LZ} for model 1 (——) and model 2 (· · · ·). Both models assume bond vector motion on the surface of a cone at an angle of 118° with respect to the symmetry axis. Note that the limiting value of S^2_{LZ} is 0.25 $(3\cos^2\theta_0 - 1)^2$, with θ_0 = 118° for both models. For model 1, S_p was calculated numerically from equations (16) and (42.1), since when $\eta/kT < 0.5$, equation (37) is not valid (see the text). S^2_{LZ} was also calculated numerically using equation (42.1), although the difference in S^2_{LZ} obtained using either equation (42.1) or (42.2) is less than 0.02.

The value of S^2_{LZ} for this particular case is given by:

$$S^2_{LZ} = (3\cos^2\theta_0 - 1)^2/4 + 6\sin^2\theta_0\cos^2\theta_0(1 - \cos\phi_0)/\phi_0^2 + 3/8\sin^4\theta_0(1 - \cos2\phi_0)/\phi_0^2 \qquad (48)$$

A plot of $[S_{QM}(j) - S_{CL}(j)]/k$ *versus* S^2_{LZ} for values of the moment of inertia, I, set to 1×10^{-46} kgm^2, 5×10^{-46} kgm^2 and 25×10^{-46} kgm^2 is shown in Figure 6b. As in the previous example, it is clear that for large values of S^2_{LZ} and for small values of I, S_{QM} and S_{CL} can be significantly different, although for $S^2_{LZ} < 0.95$,$|S_{QM} - S_{CL}|/k < 0.18$. For $S^2_{LZ} = 0.95$, $[S_{QM} - S_{CL}]/S_{QM} = 0.33$ for $I = 1 \times 10^{-46}$ kgm^2, 0.06 for $I = 5 \times 10^{-46}$ kgm^2 and 0.02 for $I = 25 \times 10^{-46}$ kgm^2. In Figure 6c and d the total value of the entropy, calculated using either classical (smooth line) or quantum mechanical (dotted line) approaches, is shown for the case of $I = 1 \times 10^{-46}$kgm^2. In Figure 6c the potential indicated in example 1 is employed while in Figure 6d the potential of example 2 is used. It is clear that $S_{QM} \geqslant 0$, while S_{CL} becomes negative for large values of S^2_{LZ}. Note that S_{CL} is no longer accurate for these values of S^2_{LZ}, since equation (10) is not valid in this limit.

The results illustrated in Figure 6 suggest that for large values of the order parameter it is necessary to consider a quantum mechanical treatment of the problem. While this is certainly the case, it must be emphasized that the point at which S_{QM} and S_{CL} diverge depends critically on the value of I. The model considered in the present example is rather simplistic in that it assumes that the N-H^N bond vector is able to rotate freely without consideration of how such motion might be affected by neighboring bonds. Because of the partial double-bond character of the carbonyl carbon–amide nitrogen bond, the motion of the N-H^N bond vector will involve concerted movement of the amide carbonyl carbon and carbonyl oxygen atoms as well. The moment of inertia of

these atoms rotating about the N-C^{α} bond is calculated to be 16×10^{-46} kgm^2, a factor of 120 times larger than the value of I for an independently rotating N-H^N bond vector. Thus, at least in these two examples, the classical and quantum mechanical treatments give similar results so long as $S^2_{LZ} \leqslant 0.95$.

Figure 7 illustrates the conformational entropy S_p (i.e. obtained using the classical approach *via* equation (16) and neglecting the kinetic energy contribution) *versus* S^2_{LZ} profile for the two examples of bond vector motion considered above. It is of interest to note that the slopes of both of the S_p curves are similar, indicating that for a given change in order parameter, reflecting a change in η or ϕ_0 in examples 1 and 2, respectively, the values of ΔS_p predicted from the two different motional models will be nearly the same. Note that for both cases the value of the order parameter can never reach zero (see equations (43) and (48)).

Acknowledgements

This research is supported by the National Cancer Institute of Canada, the National Sciences and Engineering Research Council of Canada and the Protein Engineering Center of Excellence. The authors are grateful to Professor Carmay Lim, Institute of Biomedical Sciences, Academia Sinica, Taiwan and Mr Marios Philippopoulos, University of Toronto, for sharing their 1.12 ns dynamics trajectory of RNase HI. The authors thank Professor Art Palmer, Columbia University, and Dr Shangwu Ding, University of British Columbia for a number of stimulating discussions. L. E. K. is an Alfred P. Sloan Research Fellow.

References

Akke, M. & Palmer, A. G. (1996). Monitoring macromolecular motions on microsecond to millisecond timescales by $R_{1\rho}$-R_1 constant relaxation time NMR spectroscopy. *J. Am. Chem. Soc.* **118**, 911–912.

Akke, M., Bruschweiler, R. & Palmer, A. G. (1993). NMR order parameters and free energy: an analytic approach and application to cooperative Ca^{2+} binding by calbindin D_{9k} *J. Am. Chem. Soc.* **115**, 9832–9833.

Brainard, J. R. & Szabo, A. (1981). Theory for nuclear magnetic relaxation of probes in anisotropic systems: application to cholesterol in phospholipid vesicles. *Biochemistry*, **20**, 4618–4628.

Bruschweiler, R. & Wright, P. E. (1994). NMR order parameters of biomolecules: a new analytical representation and application to the Gaussian axial fluctuation model. *J. Am. Chem. Soc.* **116**, 8426–8427.

Brooks, C. L. II, Karplus, M. & Pettit, B. M. (1988). *Proteins: A Theoretical Perspective of Dynamics, Structure, and Thermodynamics* Wiley, New York.

Chandrashekhar, I., Clore, G. M., Szabo, A., Gronenborn, A. M. & Brooks, B. R. (1992). A 500 ps molecular dynamics simulation study of interleukin-1β in water. *J. Mol. Biol.* **226**, 239-250.

Clore, G. M., Driscoll, P. C., Wingfield, P. T. & Gronenborn, A. (1990). Analysis of the backbone dynamics of interleukin 1-β using 2D inverse detected heteronuclear ^{15}N-^{1}H NMR spectroscopy. *Biochemistry*, **29**, 7387–7401.

Dayie, K. T., Wagner, G. & Lefevere, J. F. (1996). Theory and practice of nuclear spin relaxation in proteins. *Annu. Rev. Phys. Chem.* In the press.

Deverell, C., Morgan, R. E. & Strange, J. H. (1970). Studies of chemical exchange by nuclear magnetic relaxation in the rotating frame. *Mol. Phys.* **18**, 553–559.

Doog, A. J. & Sternberg, M. J. E. (1995). Sidechain conformational entropy in protein folding. *Protein Sci.* **4**, 2247–2251.

Duntz, J. D. (1995). Win some, lose some; enthalpy-entropy compensation in weak intermolecular interactions. *Chem. Biol.* **2**, 709–712.

Dzakula, Z., Westler, W. M., Edison, A. S. & Markley, J. L. (1992a). The ''CUPID'' method for calculating the continuous probability distribution of rotamers from NMR data. *J. Am. Chem. Soc.* **114**, 6195–6199.

Dzakula, Z., Edison, A. S., Westler, W. M. & Markley, J. L. (1992b). Analysis of χ1 rotamer populations from NMR data by the cupid method. *J. Am. Chem. Soc.* **114**, 6200–6207.

Dzakula, Z., Westler, W. M. & Markley, J. L. (1996). Continuous probability distribution (CUPID) analysis of potentials for internal rotations. *J. Magn. Reson. ser., B*, **111**, 109–126.

Fowler, R. & Guggenheim, E. A. (1965). *Statistical Thermodynamics*, chapts 1 and 3, Cambridge University Press, Cambridge, UK.

Farrow, N. A., Muhandiram, D. R., Singer, A. U., Pascal, S. M., Kay, C. M., Gish, G., Shoelson, S. E., Pawson, T., Forman-Kay, J. D. & Kay, L. E. (1994). Backbone dynamics of a free and a phosphopeptide-complexed Src homology 2 domain studied by ^{15}N NMR relaxation. *Biochemistry*, **33**, 5984–6003.

Farrow, N. A., Zhang, O., Forman-Kay, J. D. & Kay, L. E. (1995). Comparison of backbone dynamics of a folded and an unfolded SH3 domain existing in equilibrium in aqueous buffer, *Biochemistry*, **34**, 868–878.

Hill, T. L. (1986). *An Introduction to Statistical Thermodynamics*, Dover, New York.

Karplus, M. & Kushick, J. N. (1981). Method for estimating the configurational entropy of macromolecules. *Macromolecules*, **14**, 325–332.

Kay, L. E., Torchia, D. A. & Bax, A. (1989). Backbone dynamics of proteins as studied by nitrogen-15 inverse detected heteronuclear NMR spectroscopy: application to staphylococcal nuclease. *Biochemistry*, **28**, 8972–8979.

Kay, L. E., Muhandiram, D. R., Farrow, N. A., Aubin, Y. & Forman-Kay, J. D. (1996). Correlation between dynamics and high affinity binding in an SH2 domain interaction. *Biochemistry*, **2**, 361–368.

Kordel, J., Skelton, N. J., Akke, M., Palmer, A. G. & Chazin, W. J. (1992). Backbone dynamics of calcium-loaded calbindin D_{9k} studied by two-dimensional proton-detected NMR spectroscopy. *Biochemistry*, **31**, 4856–4866.

Lee, K. H., Xie, D., Freire, E. & Amzel, M. (1994). Estimation of changes in side chain configurational entropy in binding and folding: general methods and application to helix formation, *Proteins: Struct. Funct. Genet.* **20**, 68–84.

Levine, I. N. (1974). *Quantum Chemistry*, Allyn and Bacon, Inc., Boston.

Lipari, G. & Szabo, A. (1982a). A model-free approach to the interpretation of nuclear magnetic resonance relaxation in macromolecules. 1. Theory and range of validity. *J. Am. Chem. Soc.* **104**, 4545–4549.

Lipari, G. & Szabo, A. (1982b) A model-free approach to the interpretation of nuclear magnetic resonance

relaxation in macromolecules. 2. Analysis of experimental results. *J. Am. Chem. Soc.* **104**, 4549–4570.
McCammon, J. A. & Harvey, S. C. (1987). *Dynamics of Proteins and Nucleic Acids*, Cambridge University Press, New York.
Muhandiram, D. R., Yamazaki, T., Sykes, B. D. & Kay, L. E. (1995). Measurements of ^{2}H T_1 and $T_{1\rho}$ relaxation times in uniformly ^{13}C-labeled and fractionally ^{2}H-labeled proteins in solution. *J. Am. Chem. Soc.* **117**, 11536–11544.
Nash, L. K. (1974). *Elements of Statistical Thermodynamics*, Addison-Wesley, Reading, MA.
Nicholson, L. K., Yamazaki, T., Torchia, D. A., Grzesiek, S., Bax, A., Stahl, S. J., Kaufman, J, D., Wingfield, P. T., Lam P. Y., Jadhav, P. K., Hodge, C.N., Domaille, P. J. & Chang, C. H. (1995). Flexibility and function in HIV-I protease. *Nature Struct. Biol.* **2**, 274–279.
Nirmala, N. R. & Wagner, G. (1988). Measurements of ^{13}C relaxation times in proteins by two-dimensional heteronuclear ^{1}H-^{13}C correlation spectroscopy. *J. Am. Chem. Soc.* **110**, 7557–7558.
Nirmala, N. R. & Wagner, G. (1989). Measurements of ^{13}C spin–spin relaxation times by two-dimensional heteronuclear ^{1}H-^{13}C correlation spectroscopy. *J. Magn. Reson.* **82**, 659–661.
Palmer, A. G. (1993). Dynamic properties of proteins using NMR spectroscopy. *Curr. Opin. Biotechnol.* **4**, 385–391.
Palmer, A. G. & Case, D. A. (1992). Molecular dynamics analysis of NMR relaxation in a zinc-finger peptide. *J. Am. Chem. Soc.* **114**, 9059–9067.
Pascal, S. M., Yamazaki, T., Singer, A. U., Kay, L. E. & Forman-Kay, J. D. (1995). Structural and dynamic characterization of the phosphotyrosine binding region of a Src homology 2 domain-phosphopeptide complex by NMR relaxation, proton exchange and chemical shift approaches. *Biochemistry*, **34**, 11353–11362.
Peng, J. W. & Wagner, G. (1992). Mapping of the spectral densities of N-H bond motions in eglin c using heteronuclear relaxation experiments. *Biochemistry*, **31**, 8571–8586.
Philippopoulos, M. & Lim, C. (1995). Molecular dynamics simulation of *E. coli* ribonuclease H1 in solution: correlation with NMR and X-ray data and insights into biological functions. *J. Mol. Biol.* **254**, 771–792.
Plum, G. E. & Breslauer, K. (1995). Calorimetry of proteins and nucleic acids. *Curr. Opin. Struct. Biol.* **5**, 682–690.
Schellman, J. A. (1987). The thermodynamic stability of proteins. *Annu. Rev. Biophys. Chem.* **16**, 115–137.
Schmid, F. X. (1989). Spectral methods of characterizing protein conformation and conformational changes. In *Protein Structure; A Practical Approach* (Creighton, T. E., ed.), pp. 251–285, IRL Press, Oxford, UK.
Smith, L. A., Mark, A. E., Dobson, C. M. & van Gunsteren, W. F. (1995). Comparison of MD simulations and NMR experiments for hen lysozyme. Analysis of local fluctuations, cooperative motions, and global changes. *Biochemistry*, **34**, 10918–10931.
Stone, M. J., Fairbrother, W. J., Palmer, A. G., Reizer, J., Saier, M. H. & Wright, P. E. (1992). The backbone dynamics of the *Bacillus subtilis* glucose permease IIA domain determined from ^{15}N NMR relaxation measurements. *Biochemistry*, **31**, 4394–4406.
Szyperski, T., Luginbuhl, P., Otting, G., Guntert, P. & Wuthrich, K. (1993). Protein dynamics studied by rotating frame ^{15}N spin relaxation times. *J. Biomol. NMR*, **3**, 151–164.
van Gunsteren, W. F. (1993). Molecular dynamics studies of proteins. *Curr. Opin. Struct. Biol.* **3**, 277–281.
Viguera, A. R., Martinez, J. C., Filimonov, V. V., Mateo, P. L. & Serrano, L. (1994). Thermodynamic and kinetic analysis of the SH3 domain of spectrin shows a two-state folding transition. *Biochemistry*, **33**, 2142–2150.
Wagner, G. (1993). NMR relaxation and protein mobility. *Curr. Opin. Struct. Biol.* **3**, 748–753.
Weber, G. (1995). van't Hoff revisted: Enthalpy of association of protein subunits. *J. Phys. Chem.* **99**, 1052–1059.
Yamasaki, K., Saito, M., Oobatake, M. & Kanaya, S. (1995). Characterization of the internal motions of *Escherichia coli* ribonuclease HI by a combination of ^{15}N-NMR relaxation analysis and molecular dynamics simulations: Examination of dynamics models. *Biochemistry*, **34**, 6587–6601.
Zhang, O. & Forman-Kay, J. D. (1995). Structural characterization of folded and unfolded states of an SH3 domain in equilibrium in aqueous buffer. *Biochemistry*, **34**, 6784–6794.

Edited by P. E. Wright

(Received 30 May 1996; received in revised form 31 July 1996; accepted 19 August 1996)